Investigation of microstructure-property relantionships of magnesia-hercynite refractory composites by a refined digital image correlation technique

Imad Khlifi, Octavian Pop, Jean-Christophe Dupré, Pascal Doumalin, Marc Huger

Version of Record: https://www.sciencedirect.com/science/article/pii/S0955221919303176
Manuscript_bf0406214b98354e53884d937620c2ef

INVESTIGATION OF MICROSTRUCTURE-PROPERTY RELANTIONSHIPS OF MAGNESIA-HERCYNITE REFRACTORY COMPOSITES BY A REFINED DIGITAL IMAGE CORRELATION TECHNIQUE

Imad Khlifi [1,*], Octavian Pop[2], Jean-Christophe Dupré[3], Pascal Doumalin[3], Marc Huger [1],
[1] Univ. Limoges, CNRS, IRCER, UMR 7315, F-87000 Limoges, France
[2] Univ. Limoges, GC2D, EA 3178, F-19300 Egletons, France
[3] Univ. Poitiers, CNRS, PPRIME, UPR 3346, F- 86962 Futuroscope Chasseneuil, France

ABSTRACT

Industrial magnesia-spinel bricks destined for thermal shock applications often show more flexibility and improved crack growth resistance. Components from the spinel structure group are usually added to promote microcracking coming from thermal expansion mismatch. This leads to the development of toughening mechanisms that are very effective in improving the crack propagation resistance.

Magnesia-hercynite composites were investigated in order to highlight their fracture process, with regard to their microstructure, by using Digital Image Correlation (DIC). The direct measurement of displacement fields between digital images of the reference state and the deformed one has provided valuable information on material deformation during loading. The aim of this work was to investigate the fracture behaviour of refractories through the coupling of the Wedge Splitting Test (WST) and DIC. By using a refined DIC process transformation taking into account a discontinuity of displacement, called 2P-DIC, a more effective characterisation of the fracture behaviour was achieved.

KEY-WORDS: Refractory, Digital Image Correlation, Wedge-splitting test, Fracture behaviour, Fracture process zone

1. Introduction

Industrial refractories used for the production of clinker in cement rotary kilns have to withstand mixed solicitations consisting in temperatures as high as 1500°C in the burning zone as well as temperature gradients in the transition zone; which account for thermomechanical stresses. In addition to this, the basic environment and an atmosphere rich with alkaline salts and sulphurs leads to further increase wear in the lining due to infiltration and corrosion mechanisms. Because of these operating conditions, significant wear and crack formation can occur while in some cases the service-life of the brick is significantly reduced due to spalling. For these reasons, magnesia-based refractories are used especially due to their good corrosion resistance to basic environments. Moreover, the addition of chromite led to the improvement of the thermomechanical properties but proved to be toxic due to the cancerogenic nature of CrO_4^{2-} [1]. The use of chromite was therefore, prohibited and prompted research for substitute components capable of achieving similar or better thermomechanical performances compared to magnesia-chromite bricks.

In fact, one of the main refractory solicitations during their service life is repeated thermal cycling which can lead to thermally induced stresses within the refractory system. Therefore, thermal shock resistance is considered to be one of the key material properties for prolonging refractory service life. The evaluation of this property has always been related to so-called thermal shock parameters developed by Kingery [2] and Hasselman [3,4]. Essentially, in most industrial applications involving thermal shocks the latter approach, linking thermal shock resistance to crack propagation resistance as opposed to crack initiation resistance, serves as a basis for the design of refractories with a reduced brittleness. Such considerations have led to the development of refractories with an engineered microstructure leading to a non-linear mechanical behaviour, high specific fracture energies and low tensile strengths [5–7]. Indeed, thanks to a better control of the processing conditions [8], the microstructure of refractories can be tailored to include energy dissipating mechanisms by adjusting the composition, aggregate size and shape. In this sense, a composite approach to improve the toughness of refractories has been commonly applied.

Consequently, many studies have been conducted on the microstructure design of magnesia-based materials for cement applications through the addition of components from the spinel group such as spinel sensu stricto, hercynite, galaxite and pleonaste. The main purpose for the addition of such components is to enable an improved thermomechanical behaviour by promoting the development of a network of microcracks as a result of coefficient of thermal expansion (CTE) mismatch leading to fracture process zone (FPZ) development [9]. In comparison with pure magnesia materials, magnesia-spinel composite bricks exhibit enhanced thermal shock resistance [10] and a non-linear mechanical behaviour thanks to the CTE mismatch between the magnesia matrix and the spinel inclusions [11–13]. The presence of damage at the microstructural scale actively dissipates the elastic energy stored in the material, leading to more strain before fracture but the strength is reduced significantly at high inclusion fractions. One of the most important features in the FPZ of refractories has been highlighted by numerous authors to be related to the crack wake region where bridging phenomena occur and lead to the so-called rising R-curve behaviour [14] [15].

In hindsight, magnesia-hercynite bricks have proven to be excellent candidates for the lining of cement rotary kilns due to their excellent resistance against corrosion by alkali salts and their enhanced thermomechanical properties, especially in comparison to regular magnesia-spinel composites [16]. In fact, hercynite has been gathering more interest in recent years as an alternative flexibilising additive as many studies have highlighted the positive influence of hercynite on the sintering of refractory bricks [17] [18], the corrosion resistance [19] and thermal properties [20]. It has been observed that the presence of hercynite generally leads to an ever-evolving microstructure in the refractory system due to interdiffusion mechanisms between hercynite and magnesia at high temperatures. These diffusion mechanisms promote the formation of a spinel solid solution leading to the development of a diffusion zone around hercynite aggregates. The influence of such mechanisms on the thermomechanical behaviour and the fracture behaviour of magnesia-hercynite bricks is still not fully understood as the microstructure is marked with complex features.

From a thermomechanical point of view, materials with pre-existing damage possess interesting fracture properties that usually translate the brittle nature of single constituent ceramics into quasi-brittle composites. Thanks to advanced fracture testing methods, such as the Wedge Splitting Test (WST) [21,22], it is possible to evaluate the fracture behaviour of quasi-brittle materials such as refractories [23]. Moreover, the development of Digital Image Correlation techniques [24,25] and its recent refinements [26–28] offers the possibility of monitoring crack propagation by measuring displacement fields and subsequently analysing strain fields for fracture analysis [29–31]. Such techniques provide the means to observe process zone evolution in quasi-brittle materials, therefore adding a rich feature to standard fracture mechanical approaches.

In this article, influence of the composition of magnesia-hercynite composites on the thermomechanical properties and the subsequent fracture behaviour has been studied through the application of a refined Digital Image Correlation technique, called Two Parts-DIC (2P-DIC), coupled to the WST.

2. Materials and Methods

2.1 Materials

Pure magnesia and a set of magnesia-hercynite (MH) model composites containing different proportions of hercynite aggregates in the 1-3mm range are studied. The raw materials used in the processing of pure magnesia and, the magnesia matrix in the hercynite composite bricks, include industrial magnesia with a low iron content with grain size ranging from fines (<0.1mm) to aggregates in the 1-3 mm and 3-5 mm range. For hercynite composite materials, the addition of iron spinel $FeAl_2O_4$ (i.e Hercynite) aggregates is done in the 1-3 mm size range, therefore replacing a proportion of magnesia aggregates in the same size range. The mix is pressed at 120 MPa and then fired at 1600 °C. In this way, model materials are produced in order to simplify the microstructure of typical industrial refractories. This approach allows for a better understanding of microstructure influence on the properties of the composite systems.

The micrographs in Figure 1 give a good overview of the typical microstructure of pure magnesia and MH composites. Given the granulometric and the chemical compositions of these materials, a model composite approach can be defined in order to better apprehend their microstructure. In this sense, the matrix in MH composites is associated with monophase magnesia which includes fine and coarse magnesia grains while hercynite aggregates represent the inclusions. The resulting microstructure of MH composites after sintering is marked by coarse magnesia and hercynite aggregates as well as micro-cracks.

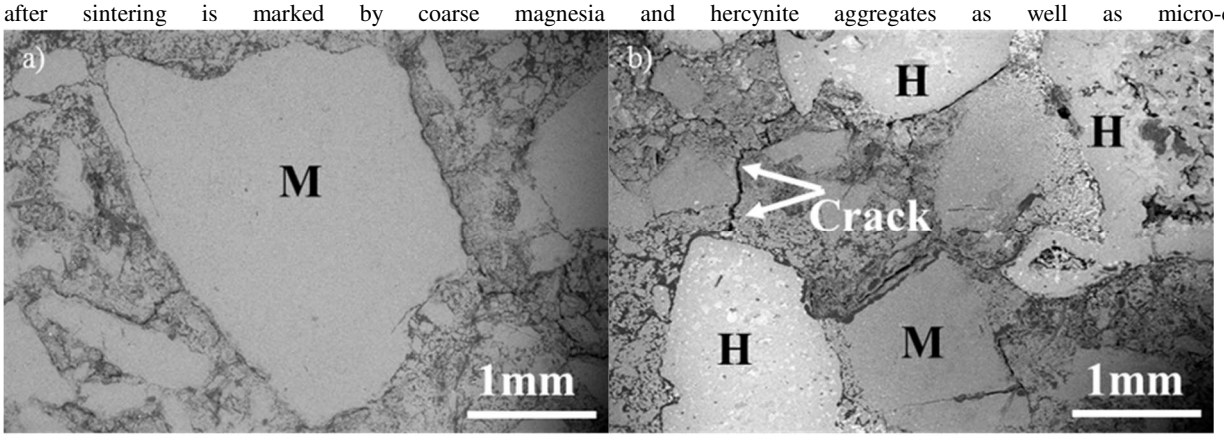

Figure 1: SEM micrograph of a) Pure MgO and b) MH composite

In fact, the thermal expansion mismatch between the magnesia matrix ($\alpha_{MgO\ (400\text{-}200°c)} = 13{,}2.10^{-6}\ °C^{-1}$) and hercynite aggregates ($\alpha_{FeAl2O4\ (400\text{-}200°c)} = 6{,}96.10^{-6}\ °C^{-1}$), leads to a thermally induced stress state that favours microcracking [32,33] during cooling after sintering, as schematised in Figure 2.a. These microcracks are likely to form networks that can act as toughening mechanisms when the material is subjected to loading. Therefore, these composites are prone to developing the so-called FPZ, as depicted in Figure 2.b, leading to an enhanced crack propagation resistance. This FPZ is composed of two main regions located at the crack tip front and behind the crack tip called the frontal process zone and the wake zone respectively. While the frontal process zone is essential in dissipating energy by development of new fracture surfaces and contributing to overall FPZ extension, it has been demonstrated [34] that the wake zone is responsible for most of the energy dissipation and to the rising R-curve phenomenon which relates directly to crack propagation resistance.

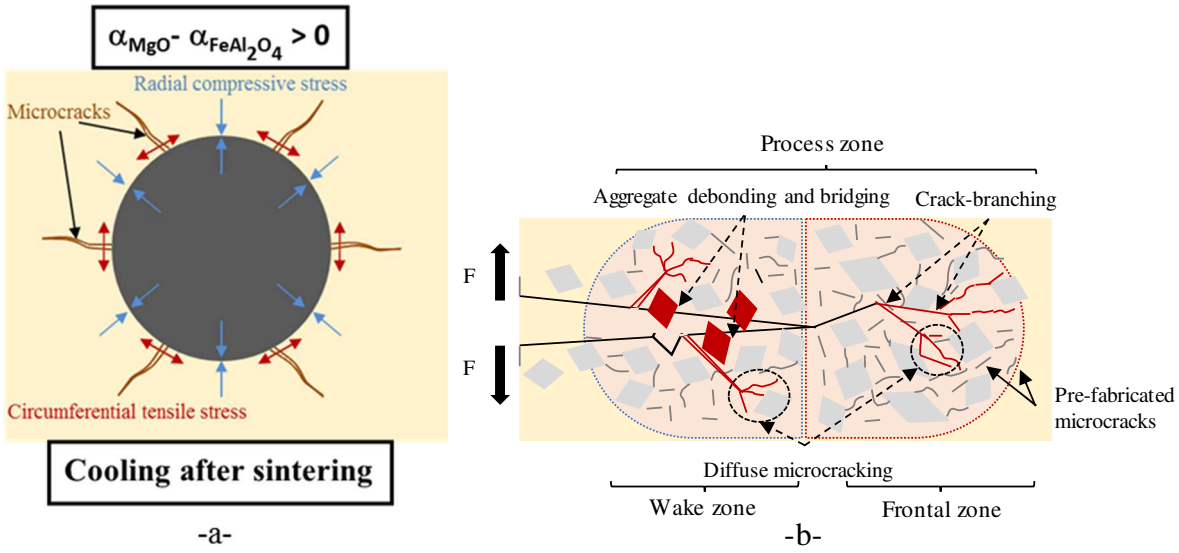

Figure 2 Schematic illustration of a) thermally induced stresses in the matrix and b) FPZ mechanisms

Samples have been machined from bricks in order to investigate the global impact of hercynite content on the thermomechanical properties and the resulting fracture behaviour of MH composites. The list of materials is presented in Table 1.

Table 1: Composition of the investigated samples

Sample	Pure MgO	MH5	MH15	MH25
Hercynite content wt. % (1-3 mm)	0%	5%	15%	25%
Bulk density (g/cm^3)	2.98	2.96	2.99	3.04
Porosity (%)	14.3%	15.4%	15.9%	15.6%

The microstructure was investigated using scanning electron microscope (SEM) observations equipped with an energy dispersive spectroscopy (EDS) probe for chemical analyses. Sample cross sections of 10x10 mm^2 were prepared according to a specific grinding and polishing protocol in order to achieve a planar surface while limiting grain debonding. Micrographs have been collected in electron back scattering mode using high vacuum in a FEI Quanta 450 FEG microscope with magnifications going up to 250x.
The identification of crystalline phases was carried out using X-ray diffraction (XRD) method on fine ground powder, with a d_{50}<10µm, of the studied materials. A Bruker D8 advanced diffractometer was used with 2θ scans going from 5° to 75° with a step of 0.01° and an exposure time of 0.475s. Sample rotation of 30 rpm and anti-scatter knife were used to improve acquisition statistics and diffraction resolution respectively.

2.2 Ultrasonic methods and acoustic emission

Ultrasonic measurements have been commonly used in the past to evaluate the elastic properties of refractories at high temperatures [35]. This low frequency method relies on using a long alumina rod as a wave-guide between the transducer and the sample, which is glued to the wave-guide using an alumina-based cement then placed in the furnace as depicted in Figure 3.a. With this technique, it is possible to evaluate Young's modulus during a thermal cycle by measuring the round-trip time for a longitudinal wave through the sample with the knowledge of its bulk density according to (1).

$$E = \rho . (\frac{2.L}{\tau})^2 \quad (1)$$

Where ρ is the bulk density of the material, L the length of the sample and τ the the round-trip time for the longitudinal wave. Tests have been performed up to 1400°C with a heating rate of 5°C/min.
Moreover, acoustic emission measurements have been performed using the same experimental conditions as for ultrasonic measurements to supplement Young's modulus evolution with information regarding microstructure evolution during the thermal cycle. In fact, as shown in Figure 3.b, this technique records acoustic signals resulting from the release of elastic energy within the sample as a result of damage mechanisms for instance. Therefore, the association of ultrasonic measurements and acoustic emission provides a good basis for establishing a link between thermomechanical properties and microstructure related events [36].

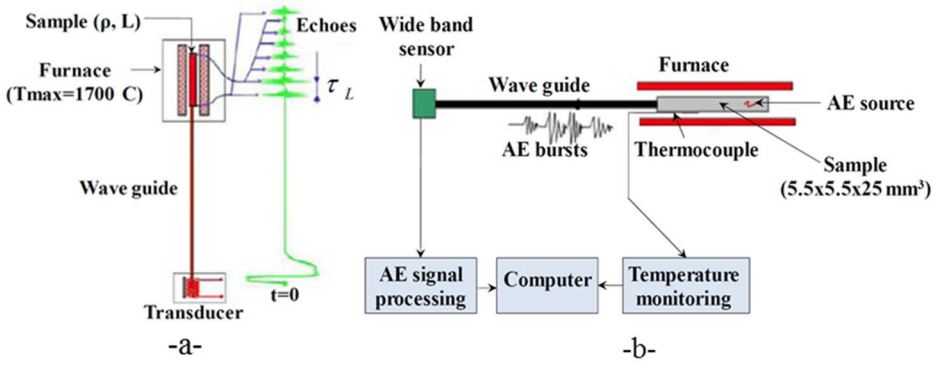

Figure 3 Experimental setup of a) ultrasonic measurement technique and b) acoustic emission **[37]**

2.3 Wedge Splitting Test (WST)

The WST provides a means to investigate the fracture behaviour of heterogeneous coarse-grained materials such as refractories. This test offers an ideal configuration to achieve stable crack propagation and measure fracture parameters such as the specific fracture energy G_f. The testing setup is composed of two metallic supports, two rolls and a wedge as shown in Figure 4.a. The load is transmitted from the wedge to the sample thanks to the metallic supports, where the vertical load F_V applied by the wedge is converted into a horizontal load F_H. This setup, made of very rigid parts, contributes to limiting the elastic energy stored in the testing machine and thus promotes stable crack propagation. Cubic samples of 100x100x100 mm^3 have been machined from refractory bricks in order to produce the groove and the starter notch for crack propagation.

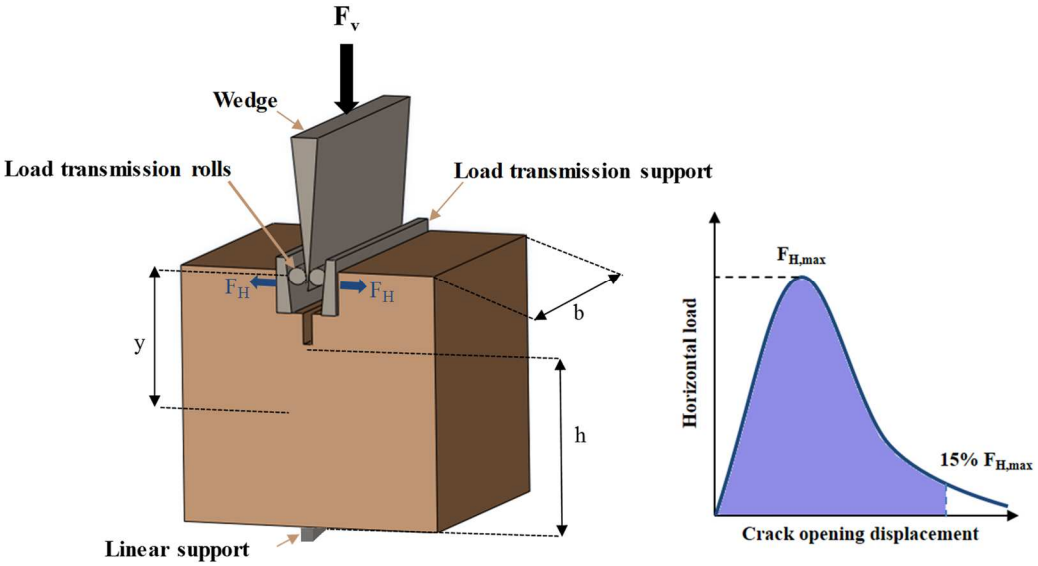

Figure 4: Illustration of WST loading setup from **[38]** and typical horizontal load-crack opening displacement curve

Loading is performed using a crosshead speed of 0.5mm/min. The applied vertical load F_V is recorded along with the crosshead vertical displacement δ_v. Then, horizontal load and crack opening displacement (COD) can be deduced from the associated vertical components using (2) and (3):

$$F_H = \frac{F_V}{2.\tan\left(\frac{\alpha}{2}\right)} \quad (2)$$

$$COD = 2.\delta_v.\tan\left(\frac{\alpha}{2}\right) \quad (3)$$

Where α, equal to 10°, is the angle of the wedge. The accurate measurement of the horizontal load and COD is a key point during WST experiments. Particularly so for the COD as crosshead displacement is usually prone to parasitic machine displacements. For this reason, this parameter is measured using digital image correlation, an optical method detailed in the following section.

From the maximum load and specimen dimensions, the nominal notch tensile strength can be calculated using equation (4):

$$\sigma_{NT} = \frac{F_{H\,max}}{b.h} + \frac{6F_{H\,max}.y}{b.h^2} \quad (4)$$

Where $F_{H\,max}$ is the maximum horizontal load, b and h are the width and the height of the fracture surface and y the vertical distance between the loadpoint and the centre of gravity of the fracture area.

The specific fracture energy can then be calculated from the total area under the horizontal load-COD curve (Figure 4.b) according to the integral in (5):

$$G_f = \frac{1}{A}\int_0^{\delta_{H\ max}} F_H \,.\, d\delta_H \qquad (5)$$

Where A is the projected fracture surface area, δ_H the COD and δ_{max} represents its maximum value during the fracture test. For practical reasons, the fracture energy is calculated up to 15% of the maximum horizontal load as shown in Figure 4.b. The specific fracture energy can be decomposed into an elastic contribution and an irreversible component, which relates to the energy consumed by the FPZ during crack propagation. Therefore, the dissipated energy is deduced from the difference between the specific fracture energy and the elastic energy, which is expressed following (6) and (7):

$$G_{el} = \frac{1}{2} F_H \delta_H \qquad (6)$$

$$G_{diss} = G_f - G_{el} \qquad (7)$$

The elastic energy is calculated at each loading state by assuming an elastic material behaviour.

2.4 Digital Image Correlation (DIC)

2.4.1 DIC application setup and refined 2P-DIC method

Digital Image Correlation (DIC) is an optical technique for displacement field measurements. It has been applied in numerous topics of experimental mechanics [39], including the study of the mechanical behaviour of refractory materials [40]. It consists in matching reference and deformed 2D images, corresponding to two different states of mechanical loading of a sample, based on their grey level distribution. The matching process is performed within a region of interest (ROI) on user-defined subsets by defining a plane material transformation ϕ between reference and successive images, where a correlation coefficient C is used to find the best values for the unknown displacement components according to an optimisation routine. The latter evaluates the resemblance of grey level distributions of pixels between initial and deformed states assuming the conservation of optical flow.

In this study, DIC has been used to monitor the COD while a refined DIC technique, named Two Parts-Digital Image Correlation (2P-DIC) has been used to investigate the propagation of vertical cracks during a WST. The 2P-DIC process uses the same principle as subset-based DIC and is detailed elsewhere in [26]. According to an optimisation method similar to that of standard DIC, this technique measures the position and rotation of a crack in addition to crack opening. Subsequently, crack presence can be determined per a user defined pseudo-strain threshold ε_s. With the refined 2P-DIC approach, the hypothesis of material discontinuity is applied to each subset and can lead to subset splitting. Therefore, an increased crack spatial resolution can be expected compared to standard DIC.

The sample surface was prepared for the DIC matching process by spraying an opaque black layer then droplets of white paint. This way, an artificial speckle pattern was created to follow material displacements. The experimental setup in Figure 5 was used to acquire images, whereby a CMOS camera was placed in front of a prepared WST sample. LED lights were used as a cold light source to provide sufficient illumination without heating the samples. The images are then processed using the DIC and 2P-DIC Correla softwares to measure the displacement fields as displayed on Figure 5 for illustrative purposes.

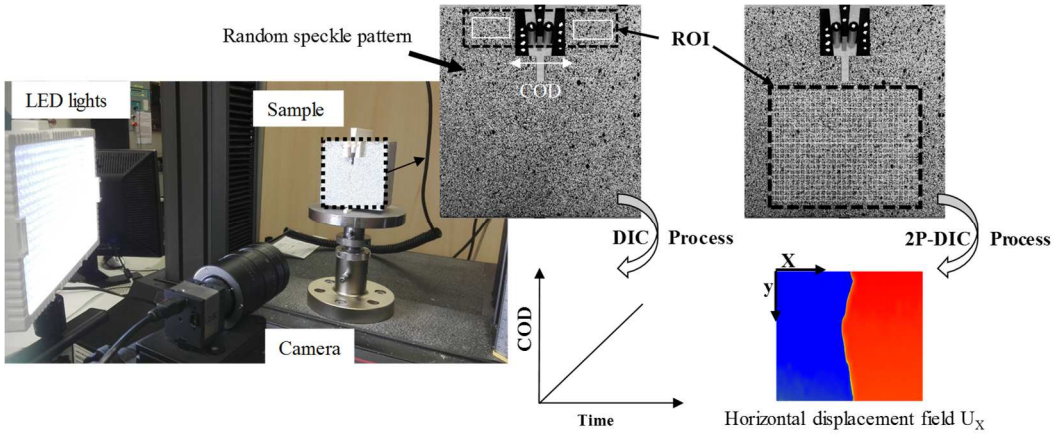

Figure 5: Experimental setup for DIC coupled with WST

The application of these correlation techniques during a WST experiment is twofold. First the measurement of COD is performed by standard DIC using large subsets on each side of the sample, as shown in Figure 5, in order to achieve high accuracy. Then, crack propagation is monitored using small overlapping subsets with dimensions of 64x16 px^2 and a spacing of 32x8 px^2

2.4.2 Crack length evaluation by 2P-DIC

The crack length is evaluated from 2P-DIC measurements by using the calculated strain field and an appropriate user-defined pseudo-strain as a threshold to discriminate cracks from noise. In fact, the threshold has a direct influence on the measured crack length as it can lead to either overestimation or underestimation of the actual length as reported in Figure 6.a. Thankfully, the

procedure used in 2P-DIC, as opposed to that of standard DIC, limits the influence of pseudo-strain threshold choice on the measured crack length. Nevertheless, the choice of a pseudo-strain threshold is not straightforward since it does not relate much to the actual material fracture strain but it is directly related to the crack tip opening displacement, which is a relevant material parameter.

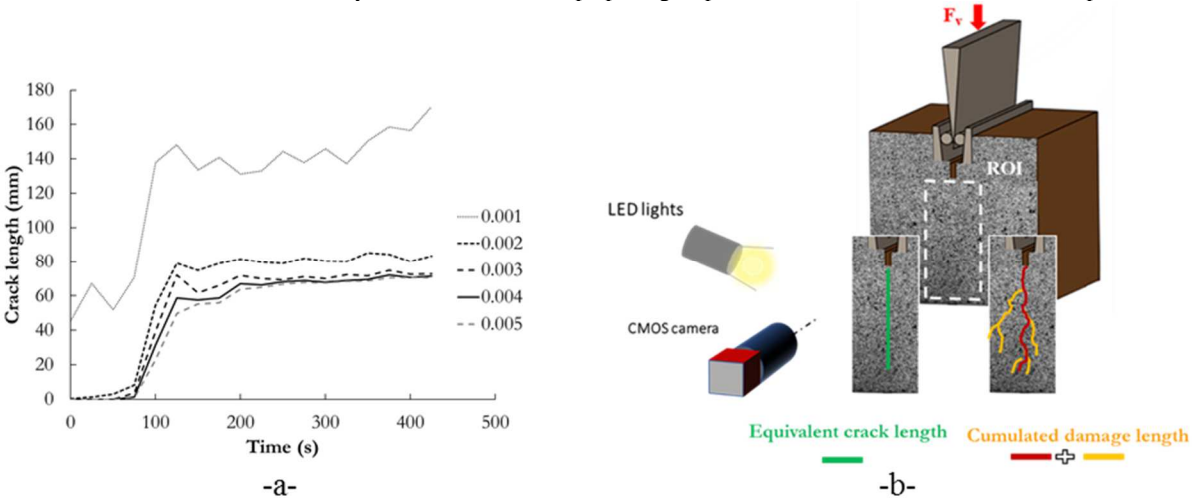

Figure 6: a) Evolution of crack length for different pseudo-strain thresholds and b) Crack length types measured by 2P-DIC

Moreover, the crack length is evaluated in two ways using 2P-DIC as shown in Figure 6.b. On one hand, it can be measured as an equivalent crack length, which corresponds to a straight line going from the notch of the sample down to the Y position of the last subset with a discontinuity. On the other hand, cumulated damage length corresponds to the sum of all vertical or inclined subset segments affected by a discontinuity. Therefore, the concept of cumulated damage length takes into account all the cracks that may have occurred during the mechanical test as long as they are within the detection limit of the camera at a specific scale. Ultimately, 2P-DIC provides ways to refine the understanding of the fracture behaviour of quasi-brittle materials.

3. Results and discussion

3.1 Microstructure characterisation

The addition of hercynite in a magnesia matrix is expected to have multiple effects on the thermomechanical behaviour, important of which is the CTE mismatch between hercynite and magnesia leading to microcrack initiation and propagation. In addition to this, SEM observations in Figure 7 shed light on large pores within hercynite and a distinguishable diffusion zone visible around the hercynite grain as bright spots appear on the magnesia matrix.

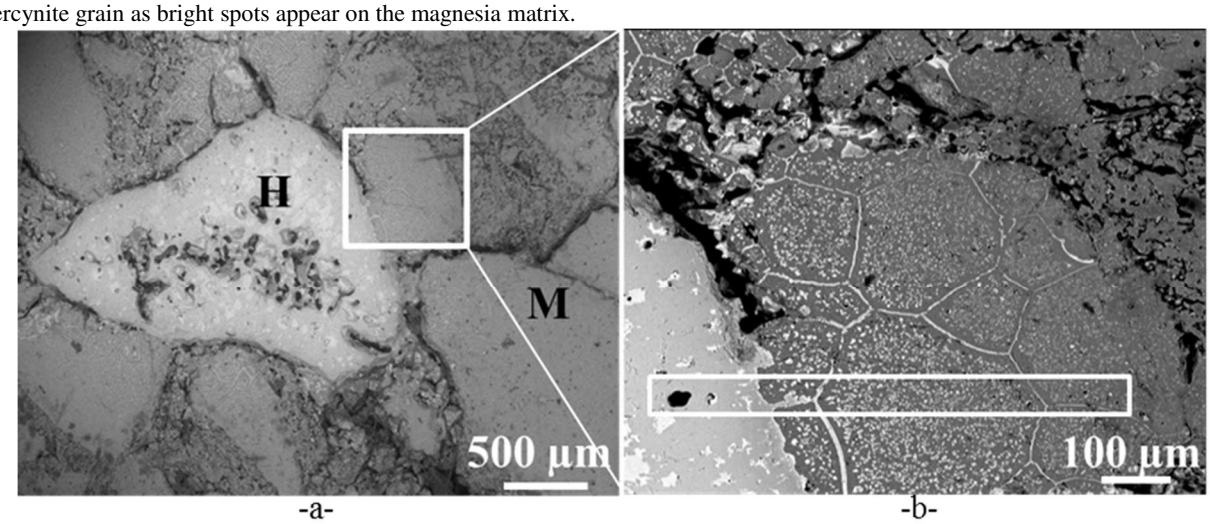

Figure 7: SEM micrograph highlighting a) a hercynite aggregate and b) the diffusion zone around hercynite

From the XRD measurements reported in Figure 8.a, it appears that a spinel solid solution had been formed as a result of high temperature interdiffusion during the sintering of the material. Furthermore, the large holes inside the hercynite grain are a possible outcome of the Kirkendall effect. This effect, reported extensively in metallic alloys and in the fabrication of hollow nanoparticles [41], points to a vacancy driven diffusion mechanism where a differential in diffusion coefficients between two atoms might exist.

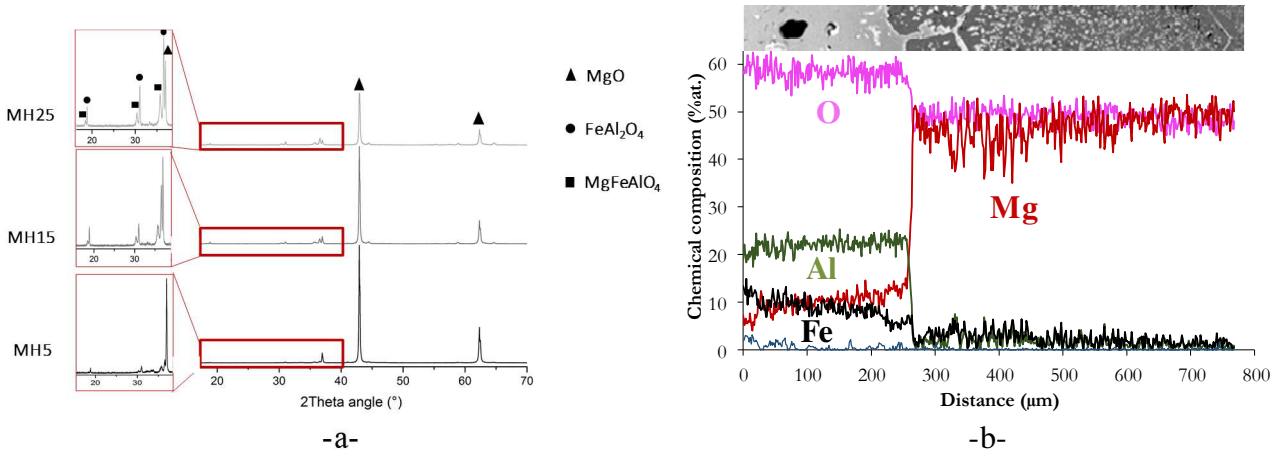

Figure 8: a) Measured XRD patterns for MH composites and b) EDS analysis of the diffusion zone

Therefore, from Figure 8.b, the presence of a diffusion zone in MH composites can be explained by the occurrence of vacancy driven interdiffusion mechanisms between magnesia and hercynite leading to Fe and Al diffusing from hercynite to magnesia and Mg from the matrix to the inclusion [42,43]. As a result, spinel solid solutions precipitate at the grain boundary and within the magnesia grains as observed in the micrograph in Figure 7.b. Additionally, the presence of large pores within hercynite hints at a potentially faster diffusion rate of iron towards magnesia. This difference in diffusion rates leads to vacancy nucleation and coalescence in the hercynite grain leaving large holes within the grain [41] [44].

Despite the presence of large pores within hercynite, the surrounding region or the so-called diffusion zone appears to be quite dense due to the precipitation of spinel solid-solutions. Therefore, spinel solid solutions within the diffusion zone might have an important impact on the thermomechanical behaviour of MH composites. In fact, these newly formed inclusions around the hercynite aggregate will most likely contribute to an increase of micromechanical stresses in the magnesia matrix during cooling due to the CTE mismatch, which in turn might increase damage occurrence within the matrix in the diffusion zone.

3.2 Thermomechanical properties

In order to evaluate the impact of hercynite content on the thermomechanical properties of MH composites, the evolution of Young's modulus was plotted as a function of temperature in Figure 9.
During the heating step, Young's modulus decreases due to the dilatation of interatomic bonds leading to a more compliant material. This behavior is generally observed for non-damaged materials such as pure MgO. For damaged materials however, such as MH composites, starting from 950°C the elastic modulus starts to increase. This increase during heating can be explained by the mechanical closure of microcracks and grain-matrix decohesions as a result of thermal expansion.

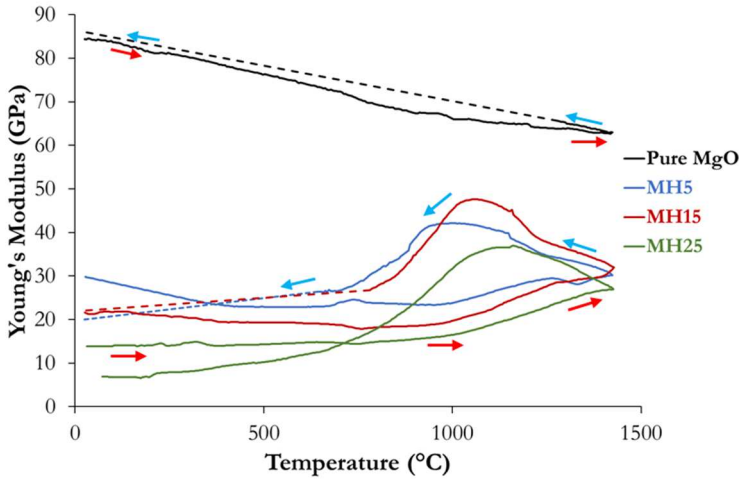

Figure 9 Evolution of Young's modulus as a function of temperature for Pure MgO and MH composites

During cooling, Young's modulus increases progressively back to its original value at room temperature for pure MgO. However, for MH composites and MH15 in particular, a steep increase in Young's modulus is observed during the first steps of cooling down to 1000°C approximately, which is followed by a strong drop. The rapid increase of Young's modulus is most likely due to the occurrence of a viscous phase acting as a crack closing aid. Conversely, further cooling leads to a significant drop in Young's modulus at a characteristic temperature for each MH composite. The reasons for this drop are strongly linked to thermally induced

stresses that stem from the CTE mismatch between hercynite and the magnesia matrix. In fact, it appears that with the addition of hercynite, the composite is likely to exhibit damage at a higher temperature during cooling, which can be explained by higher thermally induced micromechanical stresses within the matrix.
In combination with Young's modulus' measurements, the evolution of the cumulated number of acoustic emission signals is plotted as a function of temperature in Figure 10 for MH5 and MH15. As pointed by the arrows in the figure, the number of acoustic emission hits during heating is insignificant compared to those recorded during cooling. Essentially, most acoustic hits are recorded during cooling where an important rise can be noticed on the graph for MH5 and MH15, whereas pure MgO exhibits an almost negligible number of acoustic emission hits.
Indeed, this sharp increase for MH5 and MH15 occurs almost coincidentally with Young's modulus' decrease on the previous graph. Therefore, the high number of signals during cooling is presumably related to the occurrence of thermally induced microcracks coming from the CTE mismatch between magnesia and hercynite. These results demonstrate a strong correlation between thermomechanical properties and tailored microstructural features such as pre-fabricated microcracks in MH composites.

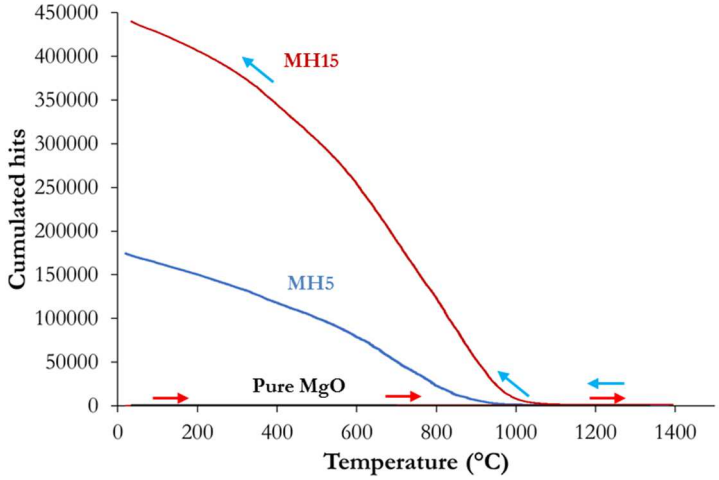

Figure 10: Acoustic emission signals as a function of temperature for Pure MgO, MH5 and MH15

Furthermore, the combination of these results underlines the microstructural mechanisms behind the hysteretic loop that drives the evolution of Young's modulus as a function of temperature, especially for MH composites. In fact, two important mechanisms are behind this hysteresis. On one hand, the diffusion driven recovery of elastic properties aided by viscous phase occurrence, during heating and the beginning of cooling. This might be a key feature of MH composites as extensive diffusion at high temperatures leads to spinel solid solution precipitation, possibly filling cracked areas. On the other hand, further cooling induces increased thermally induced stresses around hercynite aggregates leading to the cracking of the matrix and subsequent drop in elastic properties. Actually, the high number of acoustic emission hits points to a possible superimposition of stresses induced by the spinel solid solutions present within the diffusion zone as they also exhibit a CTE mismatch with the matrix.
Based on these conclusions, the impact of spinel solid-solution precipitates formed as a result of extensive diffusion around hercynite is believed to be twofold. First, the diffusion step during which the surrounding magnesia matrix is densified and constrained by precipitation of spinel solid solutions. Then, the thermally induced stress field around large and small spinel solid solutions is relaxed to generate a network of microcracks which is likely to be interconnected given the interaction of stress fields. Ultimately, at high temperatures, MH composites have a self-healing capacity driven by spinel solid solution precipitation that may lead to a better resistance to crack propagation.

3.3 Fracture behaviour

The fracture behavior of Pure MgO and MH composites has been investigated at room temperature using the WST. Horizontal Load-Displacement curves of WST have been reported in Figure 11. Pure MgO displays a rather linear elastic slope with minimal post-peak behaviour while MH composites exhibit non-linear curves as well as a rather large post-peak region.

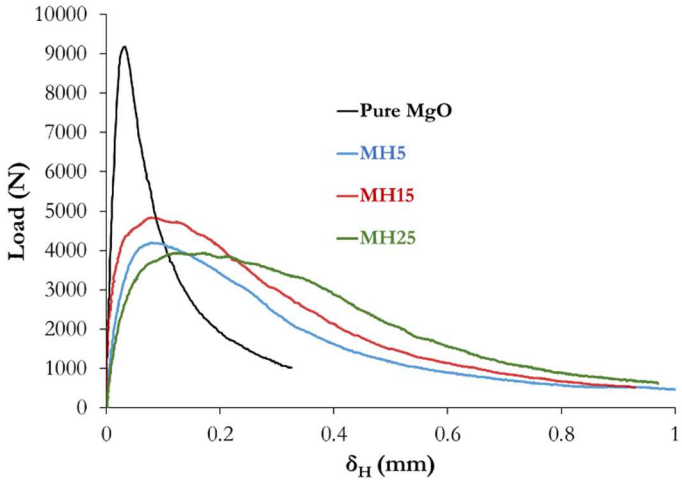

Figure 11: Horizontal load-displacement curves for Pure MgO and MH composites

Fracture energies were measured from the area under the horizontal load-displacement curves up to F_H= 15%.$F_{H\ max}$ for three samples of each material. Fracture parameters such as σ_{NT} and the G_f/σ_{NT} ratio were then computed to assess the brittleness of each material. The G_f/σ_{NT} ratio relates to material brittleness whereby a low value of the ratio indicates a brittle behaviour and vice-versa. The brittleness in this case is an evaluation of the crack propagation resistance of a material, where a reduced brittleness favours crack propagation resistance (i.e high G_f/σ_{NT} ratio).
As summarised in Table 2, Pure MgO exhibits the lowest fracture energy and the highest nominal tensile strength whereas MH composites have high fracture energies and relatively low values of nominal tensile strength. While an increasing fraction of hercynite in MH composites leads to an increase of the specific fracture energy, it does not degrade the strength of the material significantly contrarily to what could be expected, especially for MH25. In the case of MH15, the strength is on average slightly higher than that of MH5 and MH25, confirming the importance of the dual effect of hercynite addition.

This comforts the idea that hercynite and the surrounding diffusion zone participate in reducing the number of critical defects in MH composites. Thus, a good crack initiation resistance is retained, which is presumably inconvenient for optimising the crack propagation resistance.

In conjunction with these results, the G_f/σ_{NT} ratio clearly demonstrates the brittle nature of Pure MgO and the much-reduced brittleness of MH composites. The reduced brittleness of MH composites originates from their microstructure and the energy dissipating mechanisms that operate within the FPZ during crack propagation.

Table 2: Fracture parameters measured by WST

	MgO	MH5	MH15	MH25
G_f (J.m^{-2})	157.74	228.11	304.81	293.82
σ_{NT} (MPa)	9.23	4.33	4.56	4.00
G_f/σ_{NT} (µm)	17.08	52.92	66.93	73.93

In essence, the composite-like structure of MH composites along with the existence of a network of microcracks are the leading factors in developing the FPZ during crack propagation. Nevertheless, the addition of hercynite in variable amounts seems to have a dual influence on the fracture behaviour where the diffusion zone plays a key role.
While this densified zone might prove to be an obstacle to crack propagation, it is mainly improving the crack initiation resistance of MH composites according to the results obtained at room temperature. For high hercynite fractions, this might even lead to a higher crack initiation resistance at the expense of crack propagation resistance.
From a fracture point of view, the crack propagation resistance of a material is considered to be the result of a good synergy between frontal process zone phenomena and process wake. The latter drives crack propagation resistance through crack bridging while the former contributes to the overall extension of FPZ size through diffuse microcracking and crack branching
Given the previous discussion on thermomechanical-microstructure relationship and WST results, it is crucial to understand the underlying FPZ phenomena that lead to the quasi-brittle behaviour measured for MH composites.

3.4 2P-DIC analysis

For the analysis of the fracture behaviour, the 2P-DIC method has been applied to underline the main fracture mechanisms occurring in the FPZ as the crack propagates during a WST. Pure MgO and MH15 were selected for this analysis in order to appreciate the difference in terms of fracture, from a brittle material to a quasi-brittle one respectively. Sample displacement fields were measured throughout loading and calculations were performed to extract features of crack propagation from the images.

The graphs in Figure 12.a and Figure 14.a describe the evolution of the dissipated and elastic energies during loading for Pure MgO and MH15 respectively. The evolution of damage is also highlighted as the difference between the cumulated damage length and the equivalent crack length. This damage zone length represents the material's ability to develop fracture surfaces resulting from FPZ activation, namely through its frontal zone. Combined with the visualisation of 2P-DIC fields, this quantification gives an insight on the predominant frontal process zone fracture mechanisms and, to a certain extent, their subsequent influence on the total fracture energy.

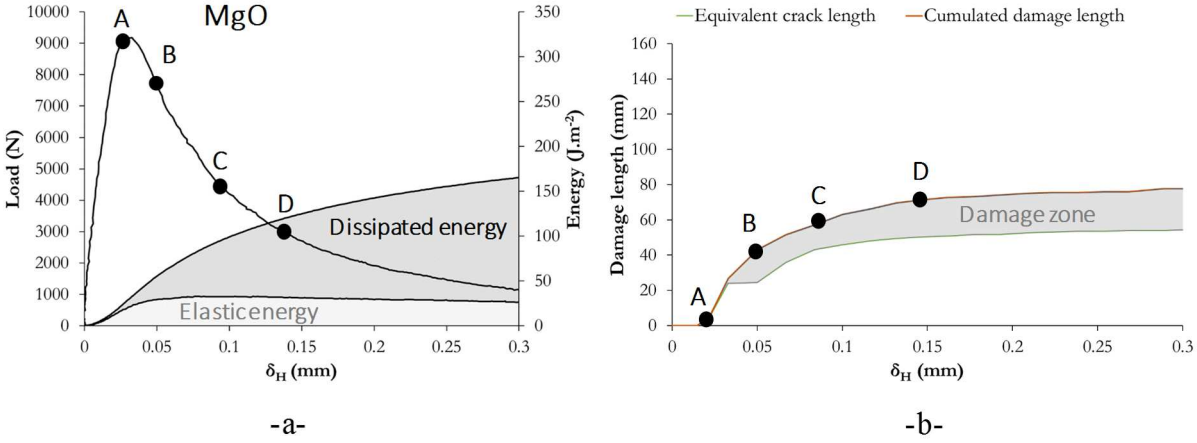

Figure 12 Fracture behaviour of Pure MgO a) Load-displacement curve and evolution of energy versus horizontal displacement, b) evolution of damage as a function of image number

As a result of 2P-DIC computations on Pure MgO, cracks were identified for a pseudo-strain threshold of ε_s=0.0015 that was selected to be just above the noise level in order to visualise all the important aspects of cracking. In this way, crack propagation was followed throughout loading as reported in Figure 13 for different loading states.

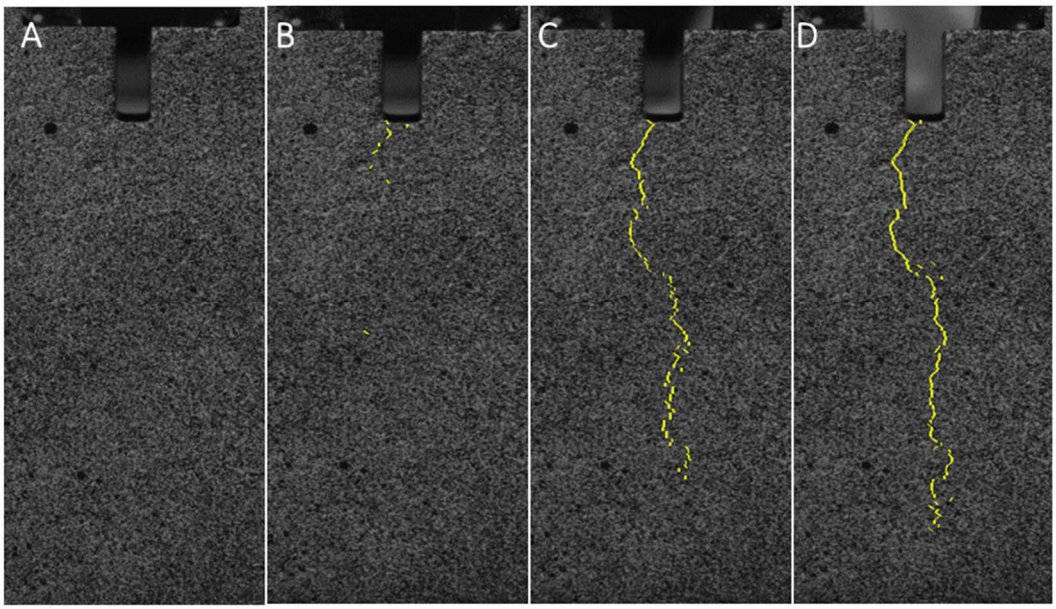

Figure 13: 2P-DIC images for Pure MgO during a WST

For Pure MgO, crack initiation occurs after the peak of the load-displacement curve as can be seen in state B. It can clearly be seen from the images in the states going from B to D that the main fracture mechanism is related to deviations of the main crack path, which can be traced back to the presence of relatively large aggregates within the microstructure of the material. Therefore, the damage zone length deduced from Figure 12.b, in this case 18mm on average, is mainly a result of crack path tortuosity. These results clearly show the presence of a FPZ in Pure MgO even though it is of limited size and therefore of limited impact.

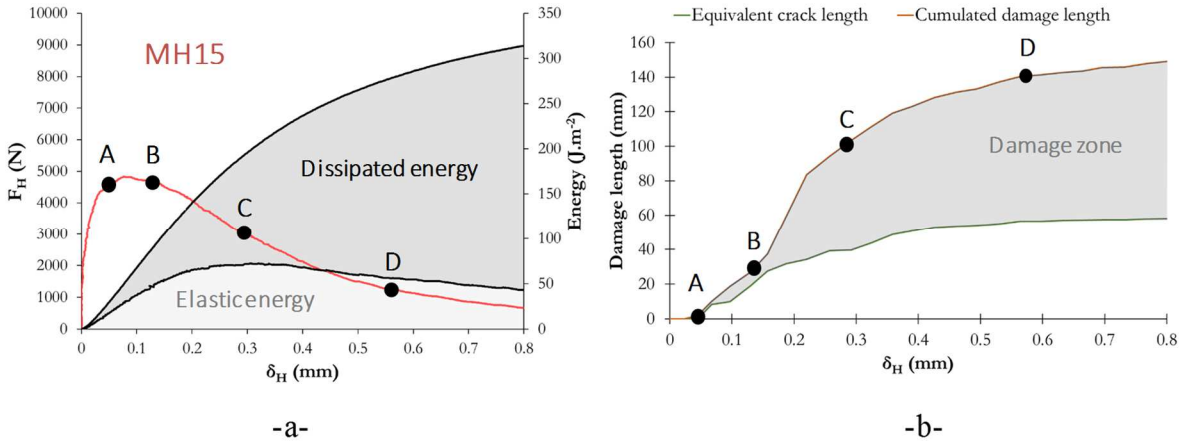

Figure 14: Fracture behaviour of MH15 a) Load-displacement curve and evolution of energy versus horizontal displacement, b) evolution of damage as a function of image number

In contrast, MH15 exhibits a much higher dissipated energy level and an extensive damage zone. From Figure 14.b, the damage zone length is estimated to be 70mm on average, which demonstrates the overall extension of the FPZ. Moreover, starting from state B in Figure 15, significant crack branching occurs with many secondary cracks. These crack branches participate directly in the dissipation of elastic energy as they contribute to the tortuosity of the crack path. Additionally, this extensive damage zone length suggests a potentially important increase in the wake region's size, which might thereafter increase the effectiveness of the FPZ in improving the crack propagation resistance.

The comparison between Pure MgO and MH15 clearly demonstrates the impact of microcracks initially engineered into the microstructure, whereby crack propagation progressively activates damage mechanisms at the crack tip and leads to further energy dissipation. In this regard, part of the energy is dissipated prior to crack initiation due to diffuse damage before localised damage takes place when a critical stress is reached locally. Therefore, these results indicate the presence of a much larger process zone size in the case of MH15.

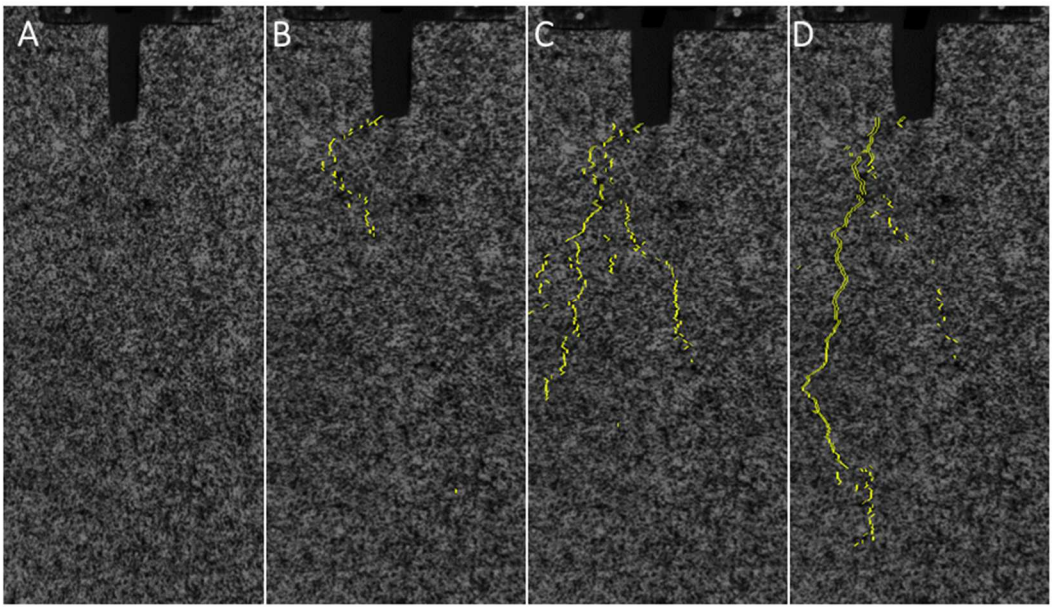

Figure 15: 2P-DIC images of MH15 during a WST

In hindsight, 2P-DIC measurements provide essential information on crack propagation but much of the information relating to the extent of process zone influence is yet to be unveiled by a single test at a fixed scale. For instance, the impact of the wake region, which is believed to be the most important part of the FPZ for increasing crack propagation resistance, is yet to be clearly demonstrated. Similarly, the impact of the diffusion zone on the fracture behaviour of MH composites is still unclear despite its significant influence on the thermomechanical properties.

4. Conclusion

The microstructure-property relationship plays a major role in understanding and improving refractory design for thermal shock applications. Indeed, throughout the investigation, microcracks resulting from the CTE mismatch between magnesia and hercynite were presented as an important feature that leads to significant thermomechanical property influence.

Essentially, the presence of hercynite in a magnesia matrix introduces several peculiarities in the microstructure, namely microcracks and diffusion zones around hercynite aggregates. As a result, the evolution of Young's modulus as a function of temperature proved to be hysteretic due to microcrack closure during heating and crack onset during cooling.

Moreover, WST experiments have shown that a reduced brittleness, characterised by a relatively high G_f/σ_{NT} ratio, was achieved for MH composites thanks to the pre-fabricated microcrack network. By the comparison of Pure MgO and MH composites, it was clearly demonstrated that the latter exhibited enhanced crack propagation resistance through increased specific fracture energy during a WST.

Finally, the application of 2P-DIC with its refined approach to fracture analysis of quasi-brittle materials proved to be valuable in understanding some key features of crack propagation. Indeed, the strain fields measured by 2P-DIC during a WST unravelled FPZ related features during crack propagation, including the crack-branching phenomenon, with an enhanced spatial accuracy.

Ultimately, the focus was directed towards MH composites due to their reported performances in thermal shock applications and their relatively complex microstructure containing microcracks and diffusion zones. The understanding of the predominant microstructural features leading to higher energy dissipation during crack propagation remains a challenge even at room temperature as complex fracture mechanisms take place. Furthermore, the extent of micro-crack and diffusion zone influence on the thermomechanical and fracture properties of hercynite-containing composites is yet to be fully understood despite recent advances in the application of optical methods to fracture mechanics.

Acknowledgements
This study was conducted within the framework of FIRE (Federation of International Refractory Research and Education) project Delta. RHI-Magnesita company is gratefully acknowledged for providing materials for the study.

REFERENCES

[1] D.J. Bray, Toxicity of Chromium Compounds Formed in Refractories, Am. Ceram. Soc. Bull. 64 (1985) 1012–1016.
[2] W.D. Kingery, Factors Affecting Thermal Stress Resistance of Ceramic Materials, J. Am. Ceram. Soc. 38 (1955) 3–15. doi:10.1111/j.1151-2916.1955.tb14545.x.
[3] D.P.H. Hasselman, Unified Theory of Thermal Shock Fracture Initiation and Crack Propagation in Brittle Ceramics, J. Am. Ceram. Soc. 52 (1969) 600–604. doi:10.1111/j.1151-2916.1969.tb15848.x.
[4] D.P.H. Hasselman, Elastic Energy at Fracture and Surface Energy as Design Criteria for Thermal Shock, J. Am. Ceram. Soc. 46 (1963) 535–540. doi:10.1111/j.1151-2916.1963.tb14605.x.
[5] G.A. Gogotsi, Ya.L. Groushevsky, K.K. Strelov, The significance of non-elastic deformation in the fracture of heterogeneous ceramic materials, Ceramurg. Int. 4 (1978) 113–118. doi:10.1016/0390-5519(78)90095-9.
[6] H. Harmuth, E.K. Tschegg, A Fracture Mechanics Approach for the Development of Refractory Materials with Reduced Brittleness, Fatigue Fract. Eng. Mater. Struct. 20 (1997) 1585–1603. doi:10.1111/j.1460-2695.1997.tb01513.x.
[7] D.R. Larson, J.A. Coppola, D.P.H. Hasselman, R.C. Bradt, Fracture Toughness and Spalling Behavior of High-Al2O3 Refractories, J. Am. Ceram. Soc. 57 (1974) 417–421. doi:10.1111/j.1151-2916.1974.tb11372.x.
[8] A.G. Evans, Perspective on the Development of High-Toughness Ceramics, J. Am. Ceram. Soc. 73 (1990) 187–206. doi:10.1111/j.1151-2916.1990.tb06493.x.
[9] M. Huger, T. Ota, N. Tessier-Doyen, P. Michaud, T. Chotard, Microstructural effects associated to CTE mismatch for enhancing the thermal shock resistance of refractories, IOP Conf. Ser. Mater. Sci. Eng. 18 (2011) 222002. doi:10.1088/1757-899X/18/22/222002.
[10] C. Aksel, B. Rand, F.L. Riley, P.D. Warren, Thermal shock behaviour of magnesia–spinel composites, J. Eur. Ceram. Soc. 24 (2004) 2839–2845. doi:10.1016/j.jeurceramsoc.2003.07.017.
[11] A. Ghosh, R. Sarkar, B. Mukherjee, S.K. Das, Effect of spinel content on the properties of magnesia–spinel composite refractory, J. Eur. Ceram. Soc. 24 (2004) 2079–2085. doi:10.1016/S0955-2219(03)00353-4.
[12] R. Grasset-Bourdel, A. Alzina, M. Huger, T. Chotard, R. Emler, D. Gruber, H. Harmuth, Tensile behaviour of magnesia-spinel refractories: Comparison of tensile and wedge splitting tests, J. Eur. Ceram. Soc. 33 (2013) 913–923. doi:10.1016/j.jeurceramsoc.2012.10.031.
[13] R. Grasset-Bourdel, A. Alzina, M. Huger, D. Gruber, H. Harmuth, T. Chotard, Influence of thermal damage occurrence at microstructural scale on the thermomechanical behaviour of magnesia–spinel refractories, J. Eur. Ceram. Soc. 32 (2012) 989–999. doi:10.1016/j.jeurceramsoc.2011.10.048.
[14] M. Sakai, J.-I. Yoshimura, Y. Goto, M. Inagaki, R-Curve Behavior of a Polycrystalline Graphite: Microcracking and Grain Bridging in the Wake Region, J. Am. Ceram. Soc. 71 (1988) 609–616. doi:10.1111/j.1151-2916.1988.tb06377.x.
[15] R.W. Steinbrech, A. Reichl, W. Schaarwächter, R-Curve Behavior of Long Cracks in Alumina, J. Am. Ceram. Soc. 73 (1990) 2009–2015. doi:10.1111/j.1151-2916.1990.tb05260.x.
[16] J. Nievoll, Z. Guo, S. Shi, Performance of magnesia hercynite bricks in large chinese cement rotary kilns, in: RHI Bull., 2006: pp. 15–17.
[17] P. Jiang, J. Chen, M. Yan, B. Li, J. Su, X. Hou, Morphology characterization of periclase–hercynite refractories by reaction sintering, Int. J. Miner. Metall. Mater. 22 (2015) 1219–1224. doi:10.1007/s12613-015-1188-6.
[18] E.A. Rodríguez, A.K. Limones, J.E. Contreras, J.J. Ruiz-Valdés, R. Puente-Ornelas, A.M. Arato, J.A. Aguilar-Martínez, Effect of hercynite spinel content on the properties of magnesia–calcium zirconate dense refractory composite, J. Eur. Ceram. Soc. 35 (2015) 2631–2639. doi:10.1016/j.jeurceramsoc.2015.03.018.
[19] J. Szczerba, I. Jastrzębska, Z. Pędzich, M. Bucko, Corrosion of Basic Refractories in Contact with Cement Clinker and Kiln Hot Meal, J. Mater. Sci. Chem. Eng. 02 (2014) 16–25. doi:10.4236/msce.2014.210003.

[20] X. Ding, H. Zhao, Z. Xiang, H. Zhang, Q. He, J. Li, Effect of hercynite content on the properties of magnesia-spinel composite refractories sintered in different atmospheres, Ceram. Int. 42 (2016) 19058–19062. doi:10.1016/j.ceramint.2016.09.063.
[21] E. Brühwiler, F.H. Wittmann, The wedge splitting test, a new method of performing stable fracture mechanics tests, Eng. Fract. Mech. 35 (1990) 117–125. doi:10.1016/0013-7944(90)90189-N.
[22] E.K. Tschegg, Test method for the determination of fracture mechanics properties, Patent specification No. A-233/86 390 328, 1986.
[23] H. Harmuth, K. Rieder, M. Krobath, E. Tschegg, Investigation of the nonlinear fracture behaviour of ordinary ceramic refractory materials, Mater. Sci. Eng. A. 214 (1996) 53–61. doi:10.1016/0921-5093(96)10221-5.
[24] H.A. Bruck, S.R. McNeill, M.A. Sutton, W.H. Peters, Digital image correlation using Newton-Raphson method of partial differential correction, Exp. Mech. 29 (1989) 261–267. doi:10.1007/BF02321405.
[25] T.C. Chu, W.F. Ranson, M.A. Sutton, Applications of digital-image-correlation techniques to experimental mechanics, Exp. Mech. 25 (1985) 232–244. doi:10.1007/BF02325092.
[26] J.-C. Dupré, P. Doumalin, Y. Belrhiti, I. Khlifi, O. Pop, M. Huger, Detection of cracks in refractory materials by an enhanced digital image correlation technique, J. Mater. Sci. 53 (2017). doi:10.1007/s10853-017-1550-3.
[27] H. Jin, H.A. Bruck, Pointwise Digital Image Correlation Using Genetic Algorithms, Exp. Tech. 29 (2005) 36–39. doi:10.1111/j.1747-1567.2005.tb00202.x.
[28] J. Réthoré, F. Hild, S. Roux, Extended digital image correlation with crack shape optimization, Int. J. Numer. Methods Eng. 73 (2008) 248–272. doi:10.1002/nme.2070.
[29] Y. Belrhiti, M. Huger, T. Chotard, O. Pop, A. Germaneau, P. Doumalin, J. Christophe Dupré, Characterization of the Mechanical Behavior of Magnesia Spinel Refractories Using Image Correlation, Int. J. Appl. Ceram. Technol. 11 (2014). doi:10.1111/ijac.12307.
[30] Y. Dai, D. Gruber, H. Harmuth, Determination of the fracture behaviour of MgO-refractories using multi-cycle wedge splitting test and digital image correlation, J. Eur. Ceram. Soc. 37 (2017) 5035–5043. doi:10.1016/j.jeurceramsoc.2017.07.015.
[31] G.L. Golewski, Measurement of fracture mechanics parameters of concrete containing fly ash thanks to use of Digital Image Correlation (DIC) method, Measurement. 135 (2019) 96–105. doi:10.1016/j.measurement.2018.11.032.
[32] Z. Li, R.C. Bradt, Micromechanical Stresses in SiC-Reinforced Al2O3 Composites, J. Am. Ceram. Soc. 72 (1989) 70–77. doi:10.1111/j.1151-2916.1989.tb05956.x.
[33] J. Selsing, Internal Stresses in Ceramics, J. Am. Ceram. Soc. 44 (1961) 419–419. doi:10.1111/j.1151-2916.1961.tb15475.x.
[34] A.G. Evans, K.T. Faber, Crack-Growth Resistance of Microcracking Brittle Materials, J. Am. Ceram. Soc. 67 (1984) 255–260. doi:10.1111/j.1151-2916.1984.tb18842.x.
[35] N. Tessier-Doyen, J.C. Glandus, M. Huger, Untypical Young's Modulus Evolution of Model Refractories at High Temperature, J. Eur. Ceram. Soc. 26 (2006) 289–295. doi:10.1016/j.jeurceramsoc.2004.10.028.
[36] T. Chotard, J. Soro, H. Lemercier, M. Huger, C. Gault, High temperature characterisation of cordierite–mullite refractory by ultrasonic means, J. Eur. Ceram. Soc. 28 (2008) 2129–2135. doi:10.1016/j.jeurceramsoc.2008.02.029.
[37] R. Grasset-Bourdel, Structure/property relations of magnesia-spinel refractories : experimental determination and simulation, thesis, Limoges, 2011. http://www.theses.fr/2011LIMO4050 (accessed February 11, 2019).
[38] Y. Belrhiti, Etude de matériaux réfractaires à comportement mécanique non linéaire par mesure de champs de déformations, thesis, Limoges, 2015. http://www.theses.fr/2015LIMO0128 (accessed February 21, 2019).
[39] F. Hild, S. Roux, Digital Image Correlation: from Displacement Measurement to Identification of Elastic Properties – a Review, Strain. 42 (2006) 69–80. doi:10.1111/j.1475-1305.2006.00258.x.
[40] Y. Belrhiti, A. Gallet-Doncieux, A. Germaneau, P. Doumalin, J.C. Dupre, A. Alzina, P. Michaud, I.O. Pop, M. Huger, T. Chotard, Application of optical methods to investigate the non-linear asymmetric behavior of ceramics exhibiting large strain to rupture by four-points bending test, J. Eur. Ceram. Soc. 32 (2012) 4073–4081. doi:10.1016/j.jeurceramsoc.2012.06.016.
[41] H.J. Fan, U. Gösele, M. Zacharias, Formation of nanotubes and hollow nanoparticles based on Kirkendall and diffusion processes: a review, Small Weinh. Bergstr. Ger. 3 (2007) 1660–1671. doi:10.1002/smll.200700382.
[42] I. Jastrzębska, J. Szczerba, A. Błachowski, P. Stoch, Structure and microstructure evolution of hercynite spinel (Fe2+ Al2 O4) after annealing treatment, Eur. J. Mineral. (2017) 62–71. doi:10.1127/ejm/2017/0029-2579.
[43] G. Liu, N. Li, W. Yan, G. Tao, Y. Li, Composition and structure of a composite spinel made from magnesia and hercynite, J. Ceram. Process. Res. 13 (2012) 480–485.
[44] X. Liang, X. Wang, Y. Zhuang, B. Xu, S. Kuang, Y. Li, Formation of CeO2−ZrO2 Solid Solution Nanocages with Controllable Structures via Kirkendall Effect, J. Am. Chem. Soc. 130 (2008) 2736–2737. doi:10.1021/ja7109629.